Zhao et al. *NPG Asia Materials* (2020) 12:5
https://doi.org/10.1038/s41427-019-0171-5

NPG Asia Materials

ARTICLE Open Access

FeO–CeO_2 nanocomposites: an efficient and highly selective catalyst system for photothermal CO_2 reduction to CO

Jiaqing Zhao[1,2,3], Qi Yang[1], Run Shi[2], Geoffrey I. N. Waterhouse[4], Xin Zhang[2], Li-Zhu Wu[2], Chen-Ho Tung[2] and Tierui Zhang[2,3]

Abstract

Solar-driven catalysis is a promising strategy for transforming CO_2 into fuels and valuable chemical feedstocks, with current research focusing primarily on increasing CO_2 conversion efficiency and product selectivity. Herein, a series of FeO–CeO_2 nanocomposite catalysts were successfully prepared by H_2 reduction of $Fe(OH)_3$-$Ce(OH)_3$ precursors at temperatures (*x*) ranging from 200 to 600 °C (the obtained catalysts are denoted as FeCe-*x*). An FeCe-300 catalyst with an Fe:Ce molar ratio of 2:1 demonstrated outstanding performance for photothermal CO_2 conversion to CO in the presence of H_2 under Xe lamp irradiation (CO_2 conversion, 43.63%; CO selectivity, 99.87%; CO production rate, 19.61 mmol h^{-1} $g_{cat}{}^{-1}$; stable operation over 50 h). Characterization studies using powder X-ray diffraction and high-resolution transmission electron microscopy determined that the active catalyst comprises FeO and CeO_2 nanoparticles. The selectivity to CO of the FeCe-*x* catalysts decreased as the reduction temperature (*x*) increased in the range of 300–500 °C due to the appearance of metallic Fe^0, which introduced an additional reaction pathway for the production of CH_4. In situ diffuse reflectance infrared Fourier transform spectroscopy identified formate, bicarbonate and methanol as important reaction intermediates during light-driven CO_2 hydrogenation over the FeCe-*x* catalysts, providing key mechanistic information needed to explain the product distributions of CO_2 hydrogenation on the different catalysts.

Introduction

Modern societies are highly dependent on fossil fuel energy for electricity generation and transportation. Combustion of fossil fuels for energy releases CO_2 into the atmosphere, thereby causing global warming and a plethora of associated environmental problems[1–3]. To curb anthropogenic CO_2 emissions, researchers are now actively exploring different catalytic approaches for converting CO_2 into fuels and valuable commodity chemicals[4–8]. As a form of CO_2 sequestration, these catalytic approaches are particularly desirable, as they can generate economic value from CO_2 (thereby transforming CO_2 into a resource rather than an environmental problem requiring mitigation)[1,4,9]. However, transforming CO_2 into other useful compounds such as CO, CH_3OH, HCOOH, CH_4, and C_{2+} hydrocarbons is challenging, requiring activation of strong C=O bonds[10]. Accordingly, the rates of CO_2 reduction via photocatalytic methods and electrocatalytic methods are currently too low to justify serious consideration from industry[11,12]. A further challenge with CO_2 reduction is achieving high selectivity for a specific product, which is highly desirable since it eliminates the need for separation of different reaction products. Most catalytic technologies for CO_2 reduction developed to date are based on hydrogenation approaches, which typically utilize the Sabatier

Correspondence: Tierui Zhang (tierui@mail.ipc.ac.cn)
[1]Key Laboratory of Synthetic and Natural Functional Molecule Chemistry of the Ministry of Education, College of Chemistry & Materials Science, Northwest University, Xi'an 710127, China
[2]Key Laboratory of Photochemical Conversion and Optoelectronic Materials, Technical Institute of Physics and Chemistry, Chinese Academy of Sciences, Beijing 100190, China
Full list of author information is available at the end of the article.

reaction ($CO_2 + 4H_2 \rightarrow CH_4 + 2H_2O$) and/or the reverse water-gas shift (RWGS, $CO_2 + H_2 \rightarrow CO + H_2O$)[3,13]. While CO_2 can be converted into CH_4 and H_2O via the Sabatier reaction, activation of CH_4 for further conversion into other higher-value chemicals requires a considerable energy input[14,15]; thus, this approach for CO_2 conversion to value-added chemicals is not practical. In comparison, the RWGS reaction creates CO, which can be used to synthesize fuels such as methanol or various hydrocarbons via Fischer-Tropsch syntheses[6,16,17]. In addition, CO can be used as a reducing agent for smelting many metals, such as iron. Therefore, the efficient conversion of CO_2 into CO offers great economic and environmental benefits for future societies, motivating efforts to develop active and selective catalyst systems for this reaction.

Industrially, the RWGS reaction is a thermal catalytic process that utilizes transition metal-based catalysts, typically Fe, Co, Ni, Mn, Cu and combinations thereof, as the active phases[18–21]. Certain precious metal catalysts, such as Pt and Au, also show good activities for the RWGS reaction[22–24], though they are not practical for industrial use due to their scarcity and susceptibility to poisoning. Similar to many other thermal catalytic processes, the RWGS reaction operates under relatively harsh reaction conditions (temperatures ranging from 400 to 700 °C and high pressures)[25], thus requiring significant energy input to achieve meaningful CO_2 conversion rates and yields of CO. Furthermore, at such high reaction temperatures, most RWGS catalysts show significant selectivity to CH_4, thus yielding a product stream that contains CO and CH_4, necessitating subsequent product separation[26]. However, lowering the reaction temperature generally improves the selectivity toward CO, though typically at the expense of a much lower CO_2 conversion[27]. Recently, researchers have begun to explore light-driven photothermal processes as a means of driving the RWGS reaction under mild reaction conditions. In photothermal catalysis, strong absorption of solar photons by the catalyst results in catalyst heating to temperatures up to 450 °C, thus allowing traditional thermal catalytic processes to occur at reasonable rates[28–30]. Recently, Ye and coworkers reported photothermal CO_2 hydrogenation to CH_4 with good efficiency and selectivity over a series of group VIII nanocatalysts[31]. Subsequently, Zhang and coworkers reported photothermal CO_2 hydrogenation to C_{2+} hydrocarbons using an alumina-supported Co–Fe alloy nanoparticle catalyst[30]. Similarly, Garcia's group demonstrated that Co@C nanocomposites showed excellent photothermal catalytic performance for CO_2 hydrogenation to C_{2+} hydrocarbons[32]. However, the photothermal RWGS reaction has received minimal attention to date, justifying a detailed investigation.

Herein, a series of novel FeO–CeO_2 nanocomposite catalysts were prepared by H_2 reduction of $Fe(OH)_3$–$Ce(OH)_3$ precursors at temperatures between 200 and 600 °C (the catalysts are denoted as FeCe-*x*, where *x* is the reduction temperature). The Fe:Ce molar ratio in the FeCe-*x* catalysts was varied from 1:2 to 3:1. The performance of the various FeCe-*x* catalysts for photothermal CO_2 hydrogenation under light excitation (Xe lamp) was then examined. An FeCe-300 catalyst with an Fe:Ce ratio of 2:1 exhibited very high selectivity for photothermal CO_2 hydrogenation to CO (Scheme 1). The catalyst, comprising FeO and CeO_2 nanoparticles, could be heated to 419 °C under Xe lamp irradiation, resulting in a CO_2 conversion of 43.63%, a CO selectivity of 99.87%, and a CO production rate of 19.61 mmol h^{-1} g_{cat}^{-1}. In situ diffuse reflectance infrared Fourier transform spectroscopy (DRIFTS) revealed that the RWGS reaction ($CO_2 + H_2 \rightarrow CO + H_2O$) occurred on the FeO component, thus accounting for the high selectivity toward CO shown by the FeCe-300 catalyst. For FeCe-*x* catalysts synthesized at higher H_2 reduction temperatures, the appearance of metallic Fe^0 enabled the Sabatier reaction ($CO_2 + 4H_2 \rightarrow CH_4 + 2H_2O$) and thus decreased the photothermal CO_2 hydrogenation selectivity toward CO. To our knowledge, the CO yield of 19.61 mmol h^{-1} g_{cat}^{-1} yield and CO selectivity of 99.87% obtained here for the FeCe-300 catalyst are the highest yet reported for solar-driven CO_2 hydrogenation. In addition, the FeCe-300 catalyst showed excellent stability during photothermal operation, with no loss in activity or change in CO selectivity detected over 50 h of testing. The results suggest that photothermal approaches can be very effective for solar-driven reduction of CO_2 to CO.

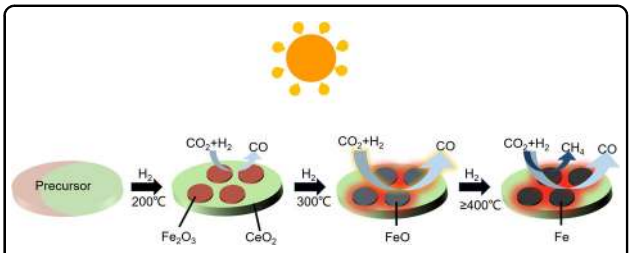

Scheme 1 Fabrication of FeCe-*x* catalysts by hydrogen reduction of $Fe(OH)_3$–$Ce(OH)_3$ precursors at 200–600 °C. The product distribution of each catalyst for CO_2 hydrogenation under light irradiation is indicated.

Materials and methods

Materials

$Ce(NO_3)_3{\cdot}9H_2O$, $Fe(NO_3)_3{\cdot}9H_2O$, commercial CeO_2, and urea were purchased from Beijing Chemical Works (Beijing, China). All the reagents were of analytical grade and used without further purification. The reaction gas mixture used in the CO_2 hydrogenation tests ($CO_2/H_2/Ar$ = 15/60/25) was purchased from Beijing Sikeda Company (Beijing, China).

Catalyst preparation

The FeCe-x nanocomposite catalysts were prepared by H_2 reduction of $Fe(OH)_3$–$Ce(OH)_3$ precursors at temperatures in the range of 200–600 °C. Briefly, precursors were prepared via a simple precipitation reaction. Typically, 0.01 mol of $Fe(NO_3)_3{\cdot}9H_2O$, 0.005 mol of $Ce(NO_3)_3{\cdot}9H_2O$ and 0.1 mol of urea were dissolved in 100 mL of deionized water. The resulting homogeneous solution was then refluxed at 110 °C for 24 h under magnetic stirring. After cooling to room temperature, the product was collected by centrifugation and washed repeatedly with deionized water and finally dried at 60 °C under vacuum. The product, a mixture of $Fe(OH)_3$ and $Ce(OH)_3$, was then transferred to a tubular furnace and reduced at different temperatures between 200 and 600 °C under a hydrogen atmosphere ($H_2/Ar = 10/90$). A heating rate of 5 °C min^{-1} was used in all experiments. The final products are denoted as FeCe-*x*, where *x* refers to the reduction temperature. For the FeCe-300 catalysts, the Fe:Ce molar was also varied to examine the effect of the Fe:Ce ratio on catalyst performance for photothermal CO_2 hydrogenation. Commercial CeO_2 with a particle size of ~50 nm was purchased from a commercial supplier and used as a reference catalyst.

Characterization

Powder X-ray diffraction (XRD) patterns for the FeCe-*x* catalysts were collected on a Bruker D8 Focus X-ray diffractometer equipped with a Cu Kα radiation source ($\lambda = 1.5405$ Å) operating at 40 kV. X-ray photoelectron spectroscopy (XPS) data were obtained on a VGESCALABMKII X-ray photoelectron spectrometer using a nonmonochromatized Al-Kα X-ray source. Transmission electron microscopy (TEM) and high-resolution TEM (HRTEM) images were collected on a JEOL-2100F microscope operating at an accelerating voltage of 200 kV. The samples were dispersed on hydrophilic carbon films for the analyses. The instrument was also equipped for high-angle annular dark-field scanning TEM (HAADF-STEM) imaging and energy-dispersive X-ray (EDX) elemental mapping. Quantitative EDX analyses were performed on a Hitachi S-4800 scanning electron microscope. UV-vis diffuse reflectance spectra were collected on a Beijing PGENERAL TU-1901 spectrometer with an integrating sphere attachment. The spectra were recorded over the wavelength range of 200–2000 nm. DRIFTS data were recorded on a Vector 70v (Brucker) infrared spectrometer with a custom-built reaction cell (as described below).

CO_2 hydrogenation tests under light irradiation

The CO_2 hydrogenation tests were carried out in a flow reaction system consisting of a Teflon-lined stainless reaction chamber (50 cm^{-3}) with a quartz window, a gas inlet and outlet, an electronic flowmeter to monitor the inlet gas flow rate and a thermocouple to measure the catalyst temperature (Figure S1, Supporting Information). For each test, 50 mg of catalyst was uniformly dispersed on a light-permeable quartz fiber filter. Next, the reaction gas mixture ($CO_2/H_2/Ar = 15/60/25$, flow rate 15 mL min^{-1}) was introduced into the reactor to achieve a pressure of 0.18 MPa. The system was then kept under these conditions for 1 h to eliminate any residual oxygen in the reactor. Then, the catalyst bed was irradiated with a 300 W Xe lamp (Beijing Perfect-light Co. Ltd, PLS-SXE-300 UV, light intensity 2.2 W cm^{-2}) to initiate photothermal CO_2 conversion. After 1 h of irradiation, a gas sample was taken from the reactor by syringe and analyzed by a Shimadzu GC-2014 chromatograph (Shimadzu Co, Japan) equipped with a three-channel analysis system. The first channel analyzed hydrocarbons in an HP PLOT Al_2O_3 column, with He as the carrier gas and a flame ionization detector (FID). The second channel analyzed CO_2, N_2, Ar, O_2, CH_4, and CO using a combination of micro packet Haysep Q, H-N and Molsieve 13× columns, employing He as the carrier gas and a thermal conductivity detector (TCD). The third channel analyzed H_2 using a micropacket HayeSep Q and Molsieve 5 Å column with N_2 as the carrier gas and a TCD detector. CO_2 conversion and product selectivity were determined by an internal standard method that used Ar. The CO yield was calculated from two standard curves with $R^2 = 0.999$.

Blank control experiments were also performed. Blank-1 tests were carried out under the same conditions as a normal test but without any catalyst. Blank-2 tests were carried out under the same conditions as a normal test but without the $CO_2/H_2/Ar = 15/60/25$ reaction gas. Both blank tests were performed after 1 h of illumination under a Xe lamp.

In situ DRIFTS studies of light-induced CO_2 hydrogenation

In situ DRIFTS was applied to study the surface intermediates formed during photothermal CO_2 hydrogenation on the different FeCe-*x* catalysts. A Vector 70v (Brucker) spectrophotometer equipped with a custom-built in situ diffuse reflectance cell was used for the DRIFTS studies. A 300 W Xe lamp was used as the light source for photothermal experiments. The in situ cell was also equipped with an electric heating device to allow specific reaction temperatures to be reached (i.e., the same temperatures that were realized in the photothermal catalytic tests). For each test, 50 mg of catalyst was loaded into the reaction cell, and a background spectrum was collected under vacuum. Subsequently, a gas mixture containing CO_2 and H_2 (v/v = 1/4) was introduced to achieve an absolute pressure of 0.18 MPa. The reaction cell was maintained in this state for 30 min to allow adsorption–desorption equilibrium to be attained. Next,

the 300 W Xe lamp and the electric heating device were applied to heat the catalyst and thus accurately simulate the temperature profiles realized in the photothermal catalytic tests. In situ DRIFTS spectra were collected every minute over a period of 1 h at 4 cm^{-1} resolution.

Results

Composition and morphology of the FeCe-*x* catalysts

The FeCe-*x* nanocomposite catalysts were prepared by H_2 reduction of a mixed hydroxide precursor with an Fe:Ce atom ratio of 2:1 (Figures S2 and S3, Supporting Information) at temperatures ranging from 200 to 600 °C. The obtained FeCe-*x* catalysts (where *x* is the reduction temperature) were characterized in detail by XRD and XPS. Figure 1a shows XRD patterns for the catalysts prepared at different reduction temperatures ($x = 200–600$ °C). The FeCe-200 catalyst showed characteristic reflections for CeO_2 (28.5, 33.1, 47.5, 56.3, and 59.1°, JCPDS-34-0394) and Fe_2O_3 (35.7 and 43.3°, JCPDS-25-1402). The data indicate that heating at 200 °C under H_2 was sufficient to transform the mixed hydroxide precursor into a mixed oxide nanocomposite. Upon increasing the reduction temperature to 300 °C, FeO (36.0 and 41.9°, JCPDS-06-0615) became the dominant Fe-containing phase. When the reduction temperature was increased above 400 °C, peaks due to metallic Fe^0 appeared (44.7 and 65.0°, JCPDS-65-4899), while the FeO peaks were attenuated, providing direct evidence for FeO reduction to Fe^0. At all reduction temperatures (*x*), CeO_2 was the dominant cerium-containing phase. The Fe 2p XPS spectra in Fig. 1b (referenced against the C 1s signal of adventitious hydrocarbons at 284.7 eV) revealed changes similar to those seen by XRD with increasing H_2 reduction temperature. At reduction temperatures up to 400 °C, only cationic Fe^{2+} and Fe^{3+} states with associated shake-up satellites were observed, consistent with the presence of FeO and Fe_2O_3, respectively. At reduction temperatures above 400 °C, new peaks appeared at low binding energies relative to the Fe^{2+}/Fe^{3+} features, which can be readily ascribed to metallic Fe^0 (e.g., Fe $2p_{3/2} = 706.7$ eV), in perfect accord with the XRD results.

UV-vis absorption spectra were collected for the FeCe-*x* catalysts to gauge their light absorption properties. Strong

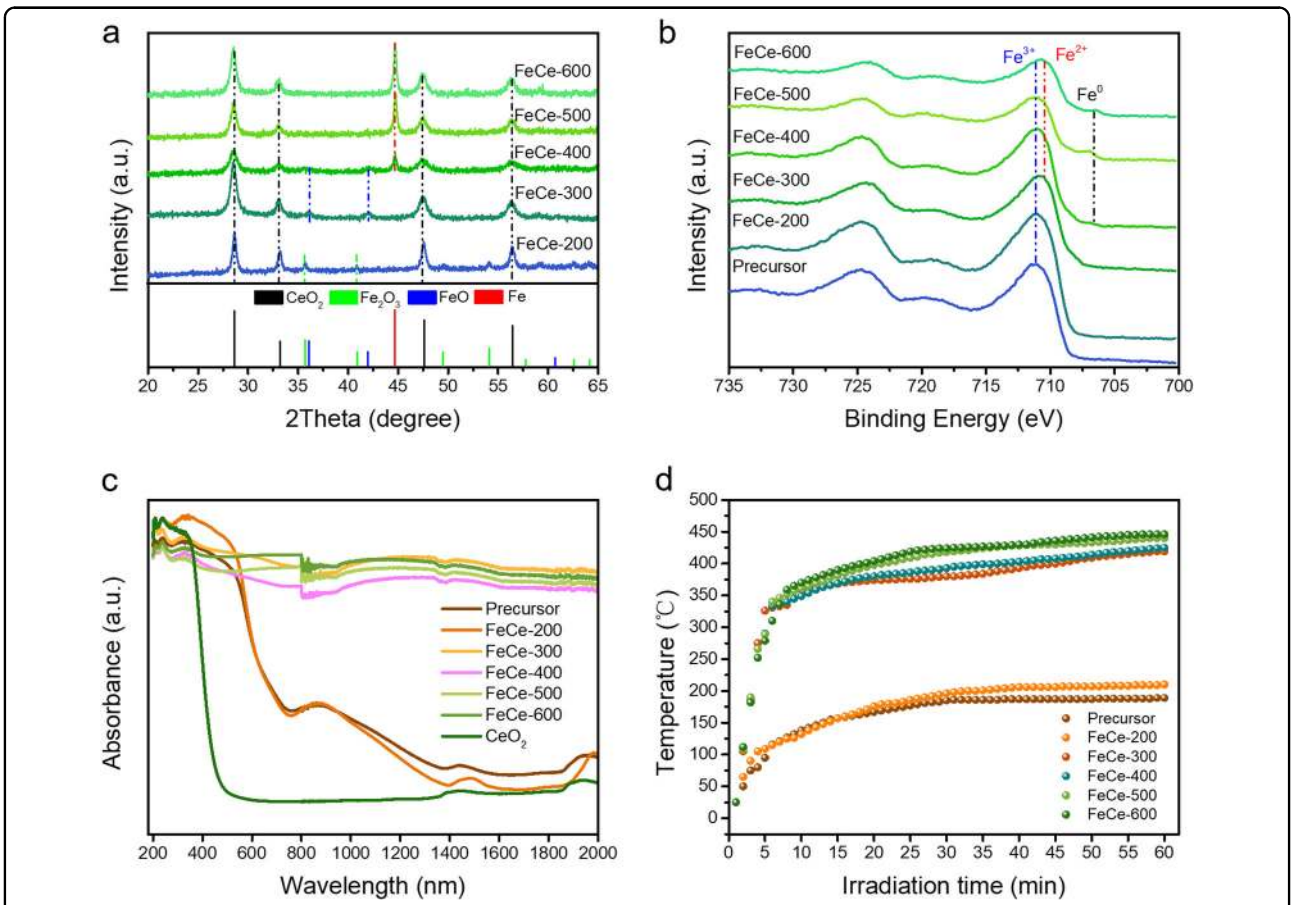

Fig. 1 a XRD patterns for the different FeCe-*x* catalysts (Fe:Ce molar ratio = 2:1). **b** Fe 2p XPS spectra for the FeCe-*x* catalysts and the FeCe hydroxide precursor. **c** UV-vis absorption spectra for the FeCe hydroxide precursor, FeCe-*x* catalysts and commercial CeO_2. **d** Catalyst surface temperature for the FeCe-*x* catalysts and FeCe hydroxide precursor under light irradiation.

absorption at UV, visible and NIR wavelengths was important to their function as photothermal catalysts for CO_2 hydrogenation (Fig. 1c). The FeCe precursor and FeCe-200 catalyst showed strong absorption below 500 nm due to the presence of Fe^{3+} and Ce^{4+} species. In contrast, the FeCe-*x* catalysts reduced at temperatures of 300 °C or above absorbed strongly from 200 to 2000 nm, indicating that they possessed excellent light absorption properties (since CeO_2 only absorbs light weakly at visible wavelengths, the strong absorption by the FeCe-*x* catalysts with $x = 300–600$ can mainly be attributed to the presence of FeO and Fe^0). In addition, the light absorption characteristics of FeCe-300 catalysts with different Fe:Ce molar ratios were also studied (Figure S4, Supporting Information). The FeCe-300 catalyst with the highest Fe:Ce molar ratio of 2:1 showed the strongest light absorption ability among the catalysts studied, again consistent with FeO rather than CeO_2 being the dominant light absorber in these nanocomposite catalysts. Next, the photothermal heating of the various FeCe-*x* catalysts under 300 W Xe lamp irradiation was examined. A thermocouple was used to monitor the surface temperature of the catalysts as a function of the irradiation time. As shown in Fig. 1d, the surface temperatures of FeCe-300, FeCe-400, FeCe-500 and FeCe-600 catalysts (Fe:Ce molar ratio 2:1) increased rapidly over the first 25 min of irradiation and then stabilized at 419, 425, 440, and 446 °C, respectively. In comparison, the photothermal heating effects for the FeCe precursor and the FeCe-200 catalyst were obviously weaker, consistent with these two samples being less effective absorbers at UV-visible-NIR wavelengths than the other FeCe-*x* catalysts.

Photothermal CO_2 hydrogenation performance

The CO_2 hydrogenation activity of the FeCe-x catalysts and selected reference catalysts (FeCe precursor and commercial CeO_2) were evaluated in a flow system under light irradiation (0.18 MPa, 15 mL min^{-1}, $CO_2/H_2/Ar = 15/60/25$) without any external heating. The results of the CO_2 hydrogenation tests are summarized in Table 1. Blank experiments showed that no hydrocarbons or CO formed in the absence of a catalyst (Blank-1) or reactant gas (Blank-2). These experiments confirmed that the reaction device did not catalyze CO_2 hydrogenation and that the catalyst itself did not decompose to produce hydrocarbons or CO. As shown in Fig. 2b and Table 1, the FeCe hydroxide precursor and FeCe-200 showed minimal activity (conversion of CO_2 <15%) for CO_2 hydrogenation under Xe lamp irradiation, which can be rationalized by their relatively weak absorption properties in the 200–2000 nm range, indicating that photothermal heating was modest (i.e., not in the ideal range for CO_2 hydrogenation). In contrast, the FeCe-300 catalyst showed remarkable activity for CO_2 hydrogenation under Xe lamp irradiation, achieving a 44.33% CO_2 conversion with an excellent selectivity toward CO of 99.87% (Fig. 2a). Upon increasing the precursor reduction temperature to 400 °C and then to 500 °C, there was no significant change in the CO_2 conversion (42.05% and 40.89%, respectively), but the CO selectivity decreased progressively (95.65% and 92.01%, respectively). When the precursor reduction temperature was increased to 600 °C, the CO_2 conversion dropped sharply to 22.75% (with CO selectivity 94.32%) due to sintering in the nanocomposite catalysts, which reduced the active area of the active Fe component. The decrease in the selectivity to CO from FeCe-300 to FeCe-500 was accompanied by a simultaneous increase in the selectivity to CH_4, with the formation of CH_4 coinciding with the appearance of Fe^0 in the catalysts (see Fig. 1). The specific CO yield for the FeCe-300 catalyst was 19.61 mmol h^{-1} $g_{cat}{}^{-1}$, higher than that obtained using any of the other FeCe-*x* catalysts. Based on this finding, we then examined the CO_2 hydrogenation performance of FeCe-300 catalysts prepared with different Fe:Ce molar ratios (Fig. 2c, Table 1). The Fe:Ce ratio of 2:1 delivered the best performance and highest CO_2 conversion among the FeCe-300 catalysts tested, reflecting its superior light absorption abilities (Figure S4, Supporting Information). Interestingly, the selectivity to CO of the various FeCe-

Table 1 CO_2 conversion and product distribution for photoinduced CO_2 hydrogenation over various FeCe-x catalysts (Fe:Ce molar ratio = 2:1), FeCe-300 catalysts with different ratios of Fe:Ce molar ratios, commercial CeO_2 and blank experiments (Blank-1: no catalyst, Blank-2: no $CO_2/H_2/Ar = 15/60/25$ reaction gas)

Entry	Catalyst	CO_2 conversion (%)	Product selectivity (%)	
			CO	CH_4
1	Blank-1	0.42	–	–
2	Blank-2	0.65	–	–
3	Precursor	9.47	98.32	1.68
4	FeCe-200	12.58	98.67	1.23
5	FeCe-300	44.33	99.87	0.13
6	FeCe-400	42.05	95.65	4.35
7	FeCe-500	40.89	92.01	7.99
8	FeCe-600	22.75	94.32	5.68
9	Fe1Ce2-300	25.42	99.92	0.08
10	Fe1Ce1-300	39.24	99.98	0.02
11	Fe2Ce1-300	43.63	99.98	0.02
12	Fe3Ce1-300	28.37	99.79	0.19
13	CeO_2	3.22	–	–

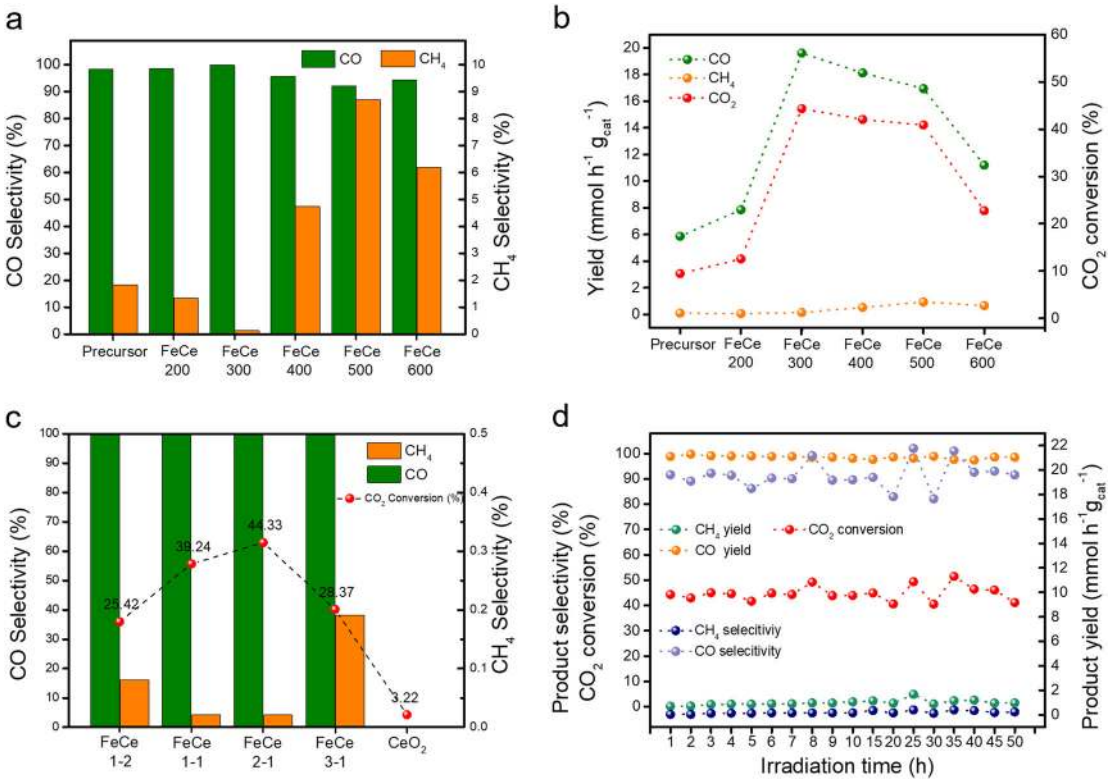

Fig. 2 a Product selectivity toward CO and CH_4 for photothermal CO_2 hydrogenation over the FeCe hydroxide precursor and FeCe-*x* catalysts (Fe:Ce molar ratio = 2:1). **b** CO_2 conversion and product yields of CH_4 and CO for the FeCe hydroxide precursor and FeCe-x catalysts. **c** CO_2 conversion and product selectivity to CH_4 and CO for FeCe-300 catalysts with different Fe:Ce molar ratios. Data for commercial CeO_2 are also shown. **d** CO_2 conversion, product yields and product selectivities over 50 h of CO_2 hydrogenation tests. Reaction conditions: 50 mg catalyst, 300 W Xenon lamp, 5 cm irradiation distance, pressure of 0.18 MPa, reaction gas composition of $CO_2/H_2/Ar = 15/60/25$.

300 catalysts was similar, consistent with all these catalysts containing the same active phase (FeO). On the basis of photothermal heating properties, CO_2 conversion, CO selectivity and CO yield, the FeCe-300 catalyst with an Fe:Ce molar ratio of 2:1 was identified as the best catalyst for CO_2 hydrogenation to CO among the various FeCe-*x* nanocomposites prepared in the current study. The results also demonstrate that the surface composition of the FeCe-x catalysts, especially the relative proportions of Fe_2O_3, FeO, and Fe^0, strongly influences the product distribution for CO_2 hydrogenation. FeO is identified as the active site for the photothermal RWGS reaction and is thus responsible for the very high CO selectivity observed for the FeCe-300 catalyst. Metallic Fe^0 promotes photothermal CO_2 hydrogenation to CH_4 and H_2O (i.e., the Sabatier reaction), thus explaining why the FeCe-400, FeCe-500, and FeCe-600 catalysts, which contain both FeO and Fe^0, afforded lower selectivities to CO than the FeCe-300 catalyst (containing only FeO).

Cycle tests of photothermal CO_2 hydrogenation were conducted on the FeCe-300 catalyst (Fe:Ce 2:1) to verify its stability. As shown in Fig. 2d, the FeCe-300 catalyst showed no significant change in CO_2 conversion (fluctuating between 40 and 52%), CO selectivity (97–99.9%) or CO yield (~20 mmol h^{-1} g_{cat}^{-1}) over 50 h of testing. The test confirmed that the FeCe-300 catalyst possessed excellent stability under the photothermal testing regime used here for CO_2 hydrogenation tests.

Morphological evolution of the FeCe-x catalysts

Since the activities and product selectivities of the FeCe-x catalysts for photothermal CO_2 hydrogenation were closely related to their surface Fe speciation, TEM and HRTEM were applied to further examine the morphologies and dispersion of FeO and Fe^0 in the catalysts. The FeCe-x catalysts all existed as nanoparticle clusters, with the mean size of the nanoparticles in the clusters increasing in size as the reduction temperature increased in the range 200–600 °C (Fig. 3a and Figure S6, Supporting Information). Obviously, increasing the reduction temperature caused nanoparticle sintering and grain growth, which was especially evident at the higher reduction temperature of 600 °C, where large FeO/Fe^0 nanoparticles were observed to form (accounting for the

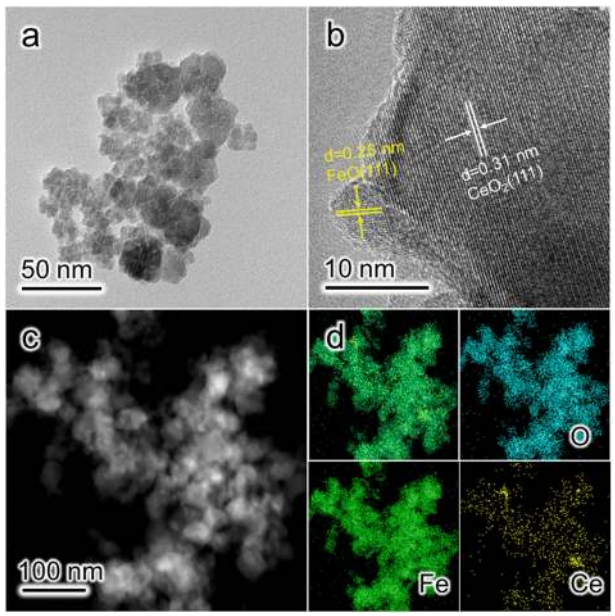

Fig. 3 Morphological characterization of the FeCe-300 catalyst (Fe:Ce molar ratio = 2:1). **a** TEM image. **b** HRTEM image. **c** HAADF-STEM image. **d** Overlayed EDS element map and individual EDS maps for O, Fe, and Ce.

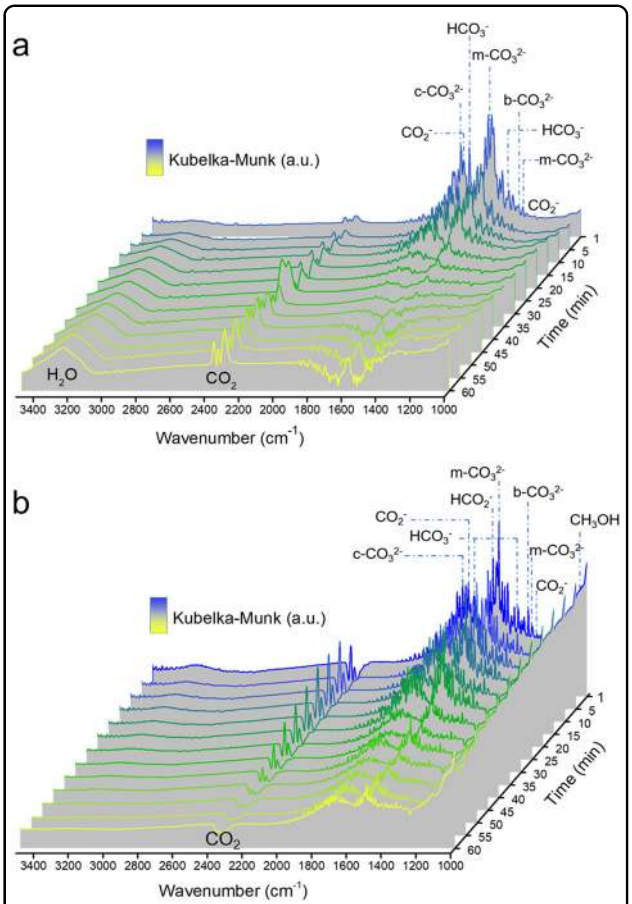

Fig. 4 In situ DRIFT spectra for photoinduced CO_2 hydrogenation on **a** FeCe-300 and **b** FeCe-500. For both catalysts, the Fe:Ce molar ratio was 2:1. The spectra were collected at a resolution of 4 cm^{-1} over a period of 1 h.

loss of the sharp drop in CO_2 conversion observed for the FeCe-600 sample during photothermal CO_2 hydrogenation tests, see Table 1). The FeCe-300 catalyst with the best CO_2 hydrogenation performance was further characterized by HRTEM, HAADF-STEM and EDX elemental mapping (Fig. 3). HRTEM lattice fringes with spacings of 0.31 and 0.25 nm were observed, corresponding to the CeO_2(111) and FeO(111) planes, respectively (Fig. 3b). EDX mapping established a very uniform distribution of Ce, Fe, O in the FeCe-300 catalyst (Fig. 3c, d), as was expected given the very small size of the FeO and CeO_2 crystallites formed at a reduction temperature of 300 °C. The identification of discrete FeO and CeO_2 nanoparticles further confirmed that the sample was indeed a nanocomposite of FeO and CeO_2 (in agreement with XRD), as opposed to a ternary oxide phase. Since pure CeO_2 demonstrated negligible CO_2 hydrogenation activity under Xe lamp irradiation, it can be concluded that the function of CeO_2 in the FeCe-x catalysts was to (1) maintain a high dispersion of active FeO and Fe^0 components and (2) act as a cocatalyst to assist with the activation of CO_2 (e.g., under photothermal reaction conditions, CeO_2 will exist as CeO_{2-x}, thus activating CO_2 adsorption through surface V_O), as suggested by other reports[33–35].

In situ DRIFTS studies of photothermal CO_2 hydrogenation

To rationalize the different selectivities of FeO and Fe^0 for photothermal CO_2 hydrogenation, in situ DRIFTS was used to identify key intermediates formed during photoinduced CO_2 hydrogenation on FeCe-300 (containing only FeO) and FeCe-500 (containing both FeO and Fe^0). For the FeCe-300 catalyst, peaks due to adsorbed CO_2, chelating bridged carbonate (c-CO_3^{2-}, 1704 cm^{-1}), monodentate carbonate (m-CO_3^{2-}, 1519 and 1315 cm^{-1}) and bidentate carbonate (b-CO_3^{2-}, 1338 cm^{-1})[36] appeared after reaction for 1 min (Fig. 4a). As the reaction proceeded, additional intermediate species, including bicarbonate (HCO_3^-, 1650 and 1423 cm^{-1}) and CO_2^- (1681 and 1268 cm^{-1})[37,38], were detected. Bicarbonate is a key intermediate in the RWGS reaction; thus, its detection here was not surprising since the FeCe-300 showed a very high selectivity for CO_2 hydrogenation to CO[38]. As the reaction continued, the characteristic peaks of adsorbed CO_2 and all the other intermediate species above decreased in intensity, indicating the consumption of these species as the reaction achieved a high steady-state rate. The development of a broad peak at 3250 cm^{-1} corresponding to adsorbed water as the reaction time approached 1 h was entirely consistent

with expectations for the RWGS ($CO_2 + H_2 \rightarrow CO + H_2O$). The DRIFTS data thus provide convincing evidence that the RWGS reaction was the dominant surface reaction on the FeCe-300 catalyst under Xe lamp irradiation, hence explaining the high selectivity of the FeCe-300 catalyst for photothermal CO_2 hydrogenation to CO (>99% selectivity). For the FeCe-500 catalyst containing FeO and Fe^0, different intermediates emerged (Fig. 4b). In the first few minutes of the reaction, three kinds of adsorbed CO_2 (1716, 1519, 1315, and 1338 cm^{-1}), a bicarbonate species (1650 and 1423 cm^{-1}), and CO_2^- (1681 and 1268 cm^{-1}) were detected. In addition, bands associated with formate (1592 cm^{-1}) and methanol (1050 cm^{-1}) appeared, which are key intermediates of the Sabatier reaction ($CO_2 + 4H_2 \rightarrow CH_4 + 2H_2O$)[38]. With increasing reaction time, the peaks associated with adsorbed CO_2, bicarbonate and CO_2^- lost intensity as was observed for FeCe-300, while the bands associated with formate and methanol were more persistent due to their continuous production and consumption. The results suggest that both the RWGS reaction and the Sabatier reaction occurred on the surface of the FeCe-500 catalyst, utilizing FeO and Fe^0 active sites, respectively. The product distributions of CO_2 hydrogenation over the FeCe-300 catalyst (RWGS pathway yielding only CO) and FeCe-500 catalyst (RWGS yielding CO and Sabatier pathway yielding CH_4) can be easily rationalized on this basis, highlighting the value of in situ DRIFTS for mechanistic assessment of working catalysts. To our knowledge, this is the one of the first occasions that DRIFTS has been successfully applied for the mechanistic investigation of a photothermal catalytic reaction.

Conclusion

In conclusion, a series of FeCe-*x* nanocomposite catalysts were successfully synthesized by a simple precipitation-reduction method. By varying the H_2 reduction temperature (*x*) in the range of 200–600 °C, the valence state of Fe in the catalysts could be adjusted from Fe_2O_3 to FeO and then Fe^0 at high temperatures (the Fe-containing phases were dispersed by CeO_2 at all temperatures). An FeCe-300 catalyst with an Fe:Ce molar ratio of 2:1 exhibited remarkable performance for photothermal CO_2 hydrogenation to CO (CO selectivity, 99.87%; CO production rate, 19.61 mmol h^{-1} g_{cat}^{-1}; and good cycling stability over 50 h). Detailed structural characterization studies and in situ DRIFTS measurements revealed that FeO in the FeCe-300 catalyst efficiently promoted the photothermal RWGS reaction, thus accounting for the very high selectivity to CO. FeCe-*x* catalysts prepared at higher reduction temperatures contained both FeO and Fe^0, the latter catalyzing the Sabatier reaction to CH_4 and thus lowering the selectivity of CO_2 hydrogenation to CO. This work identifies the photothermal RWGS reaction as a new approach for harnessing solar energy to selectively produce CO from CO_2 under mild reaction conditions.

Acknowledgements

The authors are grateful for financial support from the National Key Projects for Fundamental Research and Development of China (2018YFB1502002, 2017YFA0206904, 2017YFA0206900, 2016YFB0600901), the National Natural Science Foundation of China (51825205, 51772305, 51572270, U1662118, 21871279, 21802154), the Beijing Natural Science Foundation (2191002, 2182078, 2194089), the Strategic Priority Research Program of the Chinese Academy of Sciences (XDB17000000), the Royal Society-Newton Advanced Fellowship (NA170422), the International Partnership Program of Chinese Academy of Sciences (GJHZ1819, GJHZ201974), the Beijing Municipal Science and Technology Project (Z181100005118007), and the K. C. Wong Education Foundation. The XAFS experiments were conducted on the 1W1B beamline of the Beijing Synchrotron Radiation Facility (BSRF). G.I.N.W. acknowledges funding support from the Energy Education Trust of New Zealand, the MacDiarmid Institute for Advanced Materials and Nanotechnology, the Dodd Walls Centre for Photonic and Quantum Technologies, and the University of Auckland Faculty Research Development Fund.

Author details

[1]Key Laboratory of Synthetic and Natural Functional Molecule Chemistry of the Ministry of Education, College of Chemistry & Materials Science, Northwest University, Xi'an 710127, China. [2]Key Laboratory of Photochemical Conversion and Optoelectronic Materials, Technical Institute of Physics and Chemistry, Chinese Academy of Sciences, Beijing 100190, China. [3]Center of Materials Science and Optoelectronics Engineering, University of Chinese Academy of Sciences, Beijing 100049, China. [4]School of Chemical Sciences, The University of Auckland, Auckland 1142, New Zealand

Conflict of interest

The authors declare that they have no conflict of interest.

Supplementary information is available for this paper at https://doi.org/10.1038/s41427-019-0171-5.

Received: 2 July 2019 Revised: 27 August 2019 Accepted: 11 September 2019.
Published online: 24 January 2020

References

1. Wei, J. et al. Directly converting CO_2 into a gasoline fuel. *Nat. Commun.* **8**, 15174 (2017).
2. Zhang, J. et al. Hydrogenation of CO_2 into aromatics over a ZnCrOx-zeolite composite catalyst. *Chem. Commun. (Camb.)* **55**, 973–976 (2019).
3. Jelle, A. A. et al. Highly efficient ambient temperature CO_2 photomethanation catalyzed by nanostructured RuO_2 on silicon photonic crystal support. *Adv. Energy Mater.* **8**, 1702277 (2018).
4. Gao, P. et al. Direct conversion of CO_2 into liquid fuels with high selectivity over a bifunctional catalyst. *Nat. Chem.* **9**, 1019–1024 (2017).
5. Pan, Y. et al. Design of single-atom Co-N5 catalytic site: a robust electrocatalyst for CO_2 reduction with nearly 100% CO selectivity and remarkable stability. *J. Am. Chem. Soc.* **140**, 4218–4221 (2018).
6. Zhao, Y. et al. Reductive transformation of layered-double-hydroxide nanosheets to Fe-based heterostructures for efficient visible-light photocatalytic hydrogenation of CO. *Adv. Mater.* **30**, 1803127 (2018).
7. Xie, C. et al. Tandem catalysis for CO_2 hydrogenation to C_2-C_4 hydrocarbons. *Nano Lett.* **17**, 3798–3802 (2017).
8. Wang, L. et al. Hydrogen-treated mesoporous WO_3 as a reducing agent of CO_2 to fuels (CH_4 and CH_3OH) with enhanced photothermal catalytic performance. *J. Mater. Chem. A* **4**, 5314–5322 (2016).

9. Wang, L. et al. Incorporating nitrogen atoms into cobalt nanosheets as a strategy to boost catalytic activity toward CO_2 hydrogenation. *Nat. Energy* **2**, 869–876 (2017).
10. Song, H. et al. Light-enhanced carbon dioxide activation and conversion by effective plasmonic coupling effect of Pt and Au nanoparticles. *ACS Appl. Mater. Interfaces* **10**, 408–416 (2018).
11. Habisreutinger, S. N., Schmidt-Mende, L. & Stolarczyk, J. K. Photocatalytic reduction of CO_2 on TiO_2 and other semiconductors. *Angew. Chem. Int. Ed.* **52**, 7372–7408 (2013).
12. Qiao, J., Liu, Y., Hong, F. & Zhang, J. A review of catalysts for the electroreduction of carbon dioxide to produce low-carbon fuels. *Chem. Soc. Rev.* **43**, 631–675 (2014).
13. Gouet, A. et al. Study of the origin of the deactivation of a Pt/CeO_2 catalyst during reverse water gas shift (RWGS) reaction. *J. Catal.* **226**, 382–392 (2004).
14. Pakhare, D. & Spivey, J. A review of dry (CO_2) reforming of methane over noble metal catalysts. *Chem. Soc. Rev.* **43**, 7813–7837 (2014).
15. Liu, H. et al. Conversion of carbon dioxide by methane reforming under visible-light irradiation: surface-plasmon-mediated nonpolar molecule activation. *Angew. Chem. Int. Ed.* **54**, 11545–11549 (2015).
16. Zhou, W. et al. Direct conversion of syngas into methyl acetate, ethanol, and ethylene by relay catalysis via the intermediate dimethyl ether. *Angew. Chem. Int. Ed.* **57**, 12012–12016 (2018).
17. Zhao, B. et al. Direct transformation of syngas to aromatics over $Na\text{-}Zn\text{-}Fe_5C_2$ and hierarchical HZSM-5 tandem catalysts. *Chem* **3**, 323–333 (2017).
18. Sun, F. M., Yan, C. F., Wang, Z. D., Guo, C. Q. & Huang, S. L. Ni/Ce-Zr-O catalyst for high CO_2 conversion during reverse water gas shift reaction (RWGS). *Int. J. Hydrog. Energy* **40**, 15985–15993 (2015).
19. Williamson, D. L., Herdes, C., Torrente-Murciano, L., Jones, M. D. & Mattia, D. N-Doped Fe@CNT for combined RWGS/FT CO_2 hydrogenation. *ACS Sustain. Chem. Eng.* **7**, 7395–7402 (2019).
20. Álvarez Galván, C. et al. Reverse water-gas shift reaction at the Cu/ZnO interface: influence of the Cu/Zn ratio on structure-activity correlations. *Appl. Catal. B-Environ.* **195**, 104–111 (2016).
21. Liu, C., Cundari, T. R. & Wilson, A. K. Reaction mechanism of the reverse water-gas shift reaction using first-row middle transition metal catalysts L'M (M = Fe, Mn, Co): a computational study. *Inorg. Chem.* **50**, 8782–8789 (2011).
22. Wang, L. C., Tahvildar Khazaneh, M., Widmann, D. & Behm, R. J. TAP reactor studies of the oxidizing capability of CO_2 on a Au/CeO_2 catalyst—a first step toward identifying a redox mechanism in the Reverse Wate-Gas Shift reaction. *J. Catal.* **302**, 20–30 (2013).
23. Goguet, A., Meunier, F. C., Tibiletti, D., Breen, J. P. & Burch, R. Spectrokinetic investigation of reverse water-gas-shift reaction intermediates over a Pt/CeO_2Catalyst. *J. Phys. Chem. B* **108**, 20240–20246 (2004).
24. Roberts, G. W., Chin, P., Sun, X. & Spivey, J. J. Preferential oxidation of carbon monoxide with Pt/Fe monolithic catalysts: interactions between external transport and the reverse water-gas-shift reaction. *Appl. Catal. B-Environ.* **46**, 601–611 (2003).
25. Daza, Y. A. & Kuhn, J. N. CO_2 conversion by reverse water gas shift catalysis: comparison of catalysts, mechanisms and their consequences for CO_2 conversion to liquid fuels. *RSC Adv.* **6**, 49675–49691 (2016).
26. Bustamante, F. et al. High-temperature kinetics of the homogeneous reverse water-gas shift reaction. *AIChE J.* **50**, 1028–1041 (2004).
27. Chen, C. S., Cheng, W. H. & Lin, S. S. Study of iron-promoted Cu/SiO_2 catalyst on high temperature reverse water gas shift reaction. *Appl. Catal. A-Gen.* **257**, 97–106 (2004).
28. Zhu, X., Huo, P., Zhang, Y.-p, Cheng, D.-g & Liu, C.-j Structure and reactivity of plasma treated Ni/Al_2O_3 catalyst for CO_2 reforming of methane. *Appl. Catal. B-Environ.* **81**, 132–140 (2008).
29. Li, Z. et al. Co-based catalysts derived from layered-double-hydroxide nanosheets for the photothermal production of light olefins. *Adv. Mater.* **30**, 1800527 (2018).
30. Chen, G. et al. Alumina-supported CoFe alloy catalysts derived from layered-double-hydroxide nanosheets for efficient photothermal CO_2 hydrogenation to hydrocarbons. *Adv. Mater.* **30**, 1704663 (2018).
31. Meng, X. et al. Photothermal conversion of CO_2 into CH_4 with H_2 over Group VIII nanocatalysts: an alternative approach for solar fuel production. *Angew. Chem. Int. Ed.* **53**, 11478–11482 (2014).
32. Liu, L. et al. Sunlight-assisted hydrogenation of CO_2 into ethanol and C_{2+} hydrocarbons by sodium-promoted Co@C nanocomposites. *Appl. Catal. B-Environ.* **235**, 186–196 (2018).
33. Gamarra, D. & Martínez-Arias, A. Preferential oxidation of CO in rich H_2 over CuO/CeO_2: Operando-DRIFTS analysis of deactivating effect of CO_2 and H_2O. *J. Catal.* **263**, 189–195 (2009).
34. Wang, Y. et al. Nanocasting synthesis of chromium doped mesoporous CeO_2 with enhanced visible-light photocatalytic CO_2 reduction performance. *J. Hazard Mater.* **372**, 69–76 (2019).
35. Ju, T. J., Wang, C. H. & Lin, S. D. Insights into the CO_2 deoxygenation to CO over oxygen vacancies of CeO_2. *Catal. Sci. Technol.* **9**, 2118–2124 (2019).
36. Yin, G. et al. Hydrogenated blue titania for efficient solar to chemical conversions: preparation, characterization, and reaction mechanism of CO_2 reduction. *ACS Catal.* **8**, 1009–1017 (2018).
37. Wang, L. et al. Selective hydrogenation of CO_2 to ethanol over cobalt catalysts. *Angew. Chem. Int. Ed.* **57**, 6104–6108 (2018).
38. Wang, F. et al. Active site dependent reaction mechanism over Ru/CeO_2 catalyst toward CO_2 methanation. *J. Am. Chem. Soc.* **138**, 6298–6305 (2016).